Original Article

JCBFM

Journal of Cerebral Blood Flow & Metabolism
2018, Vol. 38(4) 697–705

DOI: 10.1177/0271678X17705042
journals.sagepub.com/home/jcbfm
SAGE

Global and multi-focal changes in cerebral blood flow during subthalamic nucleus stimulation in Parkinson's disease

Asim M Mubeen[1], Babak Ardekani[2], Michele Tagliati[3], Ron Alterman[4], Vijay Dhawan[5], David Eidelberg[5] and John J Sidtis[1]

Abstract

Electrical stimulation of subthalamic nuclei (STN) is a widely used therapy in Parkinson's disease (PD). While deep brain stimulation (DBS) of the STN alters the neurophysiological activity in basal ganglia, the therapeutic mechanism has not been established. A positron emission tomography (PET) study of cerebral blood flow (CBF) during speech production in PD subjects treated with STN-DBS found significant increases in global (whole-brain) CBF.[1] That study utilized a series of whole-slice regions of interest to obtain global CBF values. The present study examined this effect using a voxel-based principal component analysis (PCA) combined with Fisher's linear discriminant analysis (FLDA) to classify STN-DBS *on* versus STN-DBS *off* whole-brain images. The approach yielded wide-spread CBF changes that classified STN-DBS status with accuracy, sensitivity, and specificity approaching 90%. The PCA component of the analysis supported the observation of a global CBF change during STN-DBS. The FLDA component demonstrated wide-spread multi-focal CBF changes. Further, CBF measurements related to a number of subject characteristics when STN-DBS was off, but not when it was on, suggesting that the normal relationship between CBF and behavior may be disrupted by this form of neuromodulation.

Keywords

Deep brain stimulation, cerebral blood flow, subthalamic nucleus, Parkinson's disease, positron emission tomography

Received 16 September 2016; Revised 16 March 2017; Accepted 20 March 2017

Introduction

High-frequency electrical stimulation of deep brain nuclei in the basal ganglia has become a significant mode of neuro-modulatory therapy for movement disorders. For Parkinson's disease (PD), the subthalamic nucleus (STN) has been a major neurosurgical target. Although deep brain stimulation (DBS) has been effective in controlling the levodopa-responsive movement abnormalities in PD, the physiological mechanisms by which this is accomplished remain unknown.[2,3] A range of possibilities have been suggested including interference with neural signals, the desynchronization of abnormal oscillations, the alteration of inhibition and excitation within neural networks, and the modulation of neurotransmitter and hormonal signaling.[2–6] It has been recently put forward that DBS activates astrocytes, providing a mechanism for wide-spread effects in the brain.[7–9] Consistent with this suggestion, generalized increases in cerebral glucose metabolism[10] and blood flow have been reported[1] with STN-DBS. Precedents for generalized effects resulting from DBS can be found in older

[1]Brain and Behavior Laboratory, The Nathan Kline Institute for Psychiatric Research, Orangeburg, NY, USA
[2]Center for Brain Imaging and Neuromodulation, The Nathan Kline Institute for Psychiatric Research, Orangeburg, NY, USA
[3]Department of Neurology, Cedars-Sinai Medical Center, Los Angeles, CA, USA
[4]Division of Neurosurgery, Beth Israel Deaconess Medical Center, Boston, MA, USA
[5]Feinstein Center for Neurosciences, NY, USA

Corresponding author:
John J Sidtis, Brain and Behavior Laboratory, The Nathan Kline Institute for Psychiatric Research, 130 Old Orangeburg Road, Bldg 35, Orangeburg, NY 10962, USA.
Email: john.sidtis@nyu.edu

Table 1. Demographic characteristics of the subjects in the study.

ID	Age (yrs)	PD Dur (yrs)	Levodopa (mg)	DBS Dur (mos)	Left Amp (volts)	Right Amp (volts)	H&Y (off)	H&Y (on)	UPDRS III (off)	UPDRS III (on)
103	54	14	250	44	3.2	2.8	3.0	2.0	51.0	25.0
104	57	16	400	27	3.0	3.0	5.0	4.0	57.0	55.5
106	59	10	600	09	3.0	3.0	2.5	2.5	27.5	19.0
107	62	15	600	02	2.5	2.6	2.5	2.0	26.0	23.0
109	49	09	300	04	2.6	2.5	2.5	2.0	23.5	21.5
110	62	11	600	56	3.0	3.3	4.0	3.0	52.5	31.0
111	56	11	400	37	3.0	3.0	2.0	1.0	11.5	4.0

Note: All subjects were right-handed males and all but one subject were native speakers of English (106 was a native speaker of Italian who identified as a native English speaker although he immigrated to the US as an adolescent). The stimulation frequency was 185 Hz, pulse width 60 μs in all cases. The indications for STN-DBS were advanced, medically refractory PD with marked clinical swings between medication doses (i.e. *on*/*off* effects) as well as levodopa-induced dyskinesias. Both *on* and *off* evaluations were performed at least 12 h following the last dose of levodopa, which was taken the evening before the study. *On* and *off* studies were performed on different days separated by at least one week. Subject 104 had maximum scores on the rigidity items on the UPDRS III, which were not responsive to DBS. Given the uncertain washout period of DBS effects, the UPDRS *on-off* differences may underestimate the therapeutic effects. Key: Age is in years, duration of PD is in years, Levodopa is the daily dose, DBS duration is in months, left and right amplitude of STN-DBS is in volts, H&Y is the Hoehn and Yahr[38] functional status scale, UPDRS III is the Unified Parkinson's Disease Rating Scale – Motor Function.

animal studies that observed significant changes in cerebral blood flow (CBF) and blood pressure following electrical stimulation in the region of the STN.[11–15]

The present study was undertaken to further explore the characteristics of CBF changes during STN-DBS by re-examining the images previously examined using large regions of interest.[1] A principal component analysis (PCA) was used with a Fisher's linear discriminant analysis (FLDA)[16] to determine if a voxel-based pattern analysis could discriminate between STN-DBS *on* and STN-DBS *off* CBF PET scans. A potential advantage of this approach is that it does not require a priori normalization of images that are not absolutely quantitative.

Subjects and methods

Study population

Subjects have been described previously.[1] Seven, right-handed, male subjects with a mean age 57 years were recruited from a clinical population of individuals with PD who were being treated with bilateral STN-DBS. Subject characteristics are presented in Table 1. All subjects provided informed consent for the speech (The Nathan Kline Institute/Rockland Psychiatric Center Institutional Review Board; Institutional Review Board of the Mount Sinai School of Medicine) and PET (Feinstein Research Institute, Northwell Health Institutional Review Board) components of this study in accordance with the Helsinki Declaration of 1975 (and as revised in 1983).

PET imaging

A total of 166 whole-brain CBF scans were obtained from the seven subjects. Twelve whole-brain scans were obtained with STN-DBS *on* and 12 were obtained with STN-DBS *off* (one STN-DBS *off* session was terminated after 10 scans at the subject's request; accordingly, for this subject, only 10 of the *on* scans were used in this analysis). STN-DBS *on* and *off* PET scans were performed on different days, separated by at least one week. The order of the *on* and *off* scan days was randomized, with four subjects being scanned *off* first and three subjects being scanned *on* first. All subjects were studied at least 12 h after their last dose of levodopa, taken the prior evening. This levodopa washout period is routinely employed in studies on the effects of DBS.[17–19] All PET scans were performed at the Feinstein Research Institute of North Shore-Long Island Jewish Medical Center.

Subjects generally arrived at the PET suite at 8 a.m. to be consented, interviewed, and instructed in the procedures. DBS stimulation settings were recorded. All of the subjects were therapeutically stimulated 24 h/day, with the average treatment duration of 25.6 ± 21.2 months. Individual durations are listed in Table 1. Stimulators were typically turned off at 9 a.m. Approximately 30 min later, subjects were positioned in the PET scanner (GE Advance Tomograph, General Electrics) and an intraveneous line placed in the subject's left arm for $H_2{}^{15}O$ injection at 10 a.m. A stereotactic headholder and 3D laser alignment were used for stable and reproducible head positioning.

Lightweight headphones were attached to the headholder to facilitate communication with the subject. A 10-min transmission scan was performed for attenuation correction followed by a 2D PET scan to establish the delay time between $H_2{}^{15}O$ injection and the detection of brain activity by the scanner. This was followed by a series of 12 whole-brain 3D PET scans. These scans were reconstructed using 3D reprojection (3D RP) method, matrix dimensions $128 \times 128 \times 35$, with voxel dimensions of $2.34 \times 2.34 \times 4.25$ mm, and no smoothing was applied. In the DBS *off* studies, stimulation was off for an average of 61 min (minimum 40 min, maximum 86 min) prior to the first scan. The mean total duration of scanning was 85.1 ± 8.5 min in the *off* condition and 90.9 ± 10.8 min in the *on* condition. These durations were not significantly different. The average inter-scan intervals for *on* and *off* conditions did not differ either, at 8.3 and 7.6 min, respectively. Several intervals for scans occurring later in both the *on* and *off* series were longer to accommodate subjects' needs. The average dose of $H_2{}^{15}O$ injection for each scan did not differ in the DBS on and off conditions (on: 10.3 ± 1.7 mCi; off: 10.7 ± 2.1).

The scanning sequence began and ended with a resting scan. The remaining 10 scans consisted of two repetitions of five pseudorandomized speech repetition tasks (lip closure, /pa/, /pa-ta-ka/, /pop-the-top-cop/) and a spontaneous speech task in which subjects produced a monologue on a topic of their choice. These tasks were produced in random order once in the first half of the study and repeated in reverse order in the second half. Based on the observed brain delay time, each speech task was initiated 15 s prior to detection of $H_2{}^{15}O$ in the brain. Tasks were performed for 60 s using the procedure reported previously.[20] Blood flow was measured using a modified slow bolus injection of $H_2{}^{15}O$ using an automated injection system[20] and image acquisition lasted approximately 2 min. Following the PET study, all subjects underwent a protocol motor speech examination. After the speech examination, medication and STN-DBS were resumed.

Analytic method

The staff involved in data acquisition were not blinded to the DBS status. The individuals processing the data were blinded but aware of two conditions. The analysis was done directly on the PET images and not on parametric images of CBF. To classify STN-DBS images (DBS *on* versus *off condition*), we used a method that combines PCA and Fisher's linear discriminant analysis (FLDA) to determine the best discrimination pattern.[16] First, PCA performs dimensional reduction while preserving the variance in the high dimensional image space. In the next step, FLDA maximizes the distance between projected class means while at the same time minimizing the variance within a class.

PCA

PCA was used to reduce the dimensionality of the data. It provided a simplified description of imaging data by projecting the images (consisting of very high-dimensional vectors) on to the linear space spanned by the eigenvectors of the data covariance matrix.[21] We have N number of PET scans and each scan consists of P number of voxels constructing a big dimensional space of size $N \times P$. We performed PCA on this data as follows:

We restructured each image into a one dimensional vector of size $1 \times P$ and then arranged all N images into a data matrix of $N \times P$ dimensions as follows

$$\mathbf{X} = \left[x_1^i, x_2^i, x_3^i, \ldots, x_N^i\right]^T \tag{1}$$

where $i = 1, 2, 3, \ldots, P$

After mean correcting the data $\mathbf{X}$, we used singular value decomposition (SVD) to obtain a set of basis vector. The SVD of vector $\mathbf{X}$ is given by

$$\mathbf{X} = U\Sigma^{1/2}V^T \tag{2}$$

where $\sum$ is a diagonal matrix containing the $(N-1)$ eigenvalues of $\mathbf{X}$ as diagonal elements. U is orthogonal matrix of size $N \times (N-1)$. V^T is an orthogonal matrix of size $(N-1) \times P$.

U and $\sum$ can be found by PCA of an $N \times N$ matrix $\mathbf{XX^T}$ using

$$\mathbf{X}\mathbf{X}^T = U\Sigma U^T \tag{3}$$

V^T can be found from the following equation

$$V^T = \Sigma^{-1/2}U^T\mathbf{X} \tag{4}$$

Finally, the coordinates of the N PET images in the $(N-1)$-dimensional feature space can be represented by a new matrix Z that is given by

$$Z = U\Sigma^{1/2} \tag{5}$$

Z is a matrix of size $N \times (N-1)$ representing the reduced dimensional feature space. By substituting the Z in equation (2), one can return to image space.

Fisher's linear discriminant analysis

FLDA finds the optimal direction in the feature space to classify the data. FLDA is used to classify STN-DBS

on and *off* states using the reduced dimensional space Z, the product of PCA. Let $\boldsymbol{a}$ be an optimal unit vector in the feature space that optimally classifies the data. This vector is known as Fischer's discriminant vector. Let y be the projection of Z in the direction of $\boldsymbol{a}$ that is

$$y = \boldsymbol{a}^T Z \tag{6}$$

FLDA maximizes a ratio of ''between-class variance'' to ''within-class variance'' to reduce the data variation in the same class and to increase the separation between classes to determine the unit vector $\boldsymbol{a}$. This ratio is expressed as

$$argmax_a(J_a) = \frac{N_1(m_1 - m)^2 + N_2(m_2 - m)^2}{\sum_{j=1}^{N_1}(y_j - m_1)^2 + \sum_{j=1}^{N_2}(y_j - m_2)^2} \tag{7}$$

where N_1 and N_2 are the number of STN-DBS *off* and *on* images, respectively, and $m_k = \frac{1}{N_k}\sum_{y \in C_k} y$.

After obtaining the optimized direction $\boldsymbol{a}$ in the feature space $\boldsymbol{Z}$, the discriminating image $\boldsymbol{I_a}$ can be obtained using the relationship

$$\boldsymbol{I_a} = V\boldsymbol{a} \tag{8}$$

This image $\boldsymbol{I_a}$ presents the spatial pattern that best separates the two classes (STN-DBS *on* or *off*) in terms of the FLDA criterion.

To classify a given test image after the training step, a prediction value was calculated. First we projected a given test image X_T to a feature space using

$$\mathbf{Z}_P = X_T V \tag{9}$$

where $\mathbf{Z}_P$ was the projection of test image X_T to the feature space. The value of the predictor Q was calculated by using feature vectors corresponding to a number of principal components and the vector $\mathbf{a}$ pointing in the direction that maximized the Fischer's criterion. The following equation was used to find the predictor value.

$$Q = \mathbf{Z}_P\mathbf{a} \tag{10}$$

The predictor Q is used to classify the test image. Details of image processing are presented in the following section.

Image processing

PET images were first aligned within subject and then spatially normalized to a standard space using the SPM5 software (SPM5, London, UK http://www.fil.ion.ucl.ac.uk/spm/). In the first step, intra-subject rigid-body alignment was performed on the raw PET images to correct for head movement. All images were registered to the first image of the series for each subject. Mean images for each subject were estimated and then nonlinearly normalized to a PET template to reduce anatomic variability. In order to establish a template for skull-stripping individual PET scans, a mean image of all 164 scans was created using SPM5 and templates were manually drawn on the mean image slices using 'fslview' software. All images were skull-stripped using SPM5 and the manually generated template.

We used half (82 out of 164) images for training purposes and the rest for testing. The training and testing images were randomly selected. A PCA was applied to the spatially normalized, intra-subject registered, and skull-stripped images. A total of $N - 1$ (81) principal components were calculated.

PCA of the PET images can provide important information about the underlying covariance structure. It has been reported in intra-subject and inter-subject studies that the discriminating pattern is usually contained in the first principal component of intra-subject subspace.[22] However, Ardekani et al.[16] noted that the pattern that discriminates between experimental conditions can be spread into several components. We used PCA to reduce the dimensionality in our data. To reduce the noise along with the dimensionality, we selected the first 30 components for further analysis. FLDA was used to discriminate STN-DBS *on* from STN-DBS *off* scans. The FLDA analysis was repeated 10 times using different, randomly selected, training and testing sets of data. We built in-house software to implement PCA and FLDA using MATLAB 7.

The accuracy, precision, sensitivity, and specificity of the predictions made by FLDA were calculated using the following equations

$$Accuracy = \frac{TP + TN}{TP + TN + FP + FN} \tag{11}$$

$$Precision = \frac{TP}{TP + FP} \tag{12}$$

$$Sensitivity = \frac{TP}{TP + FN} \tag{13}$$

and

$$Specificity = \frac{TN}{TN + FP} \tag{14}$$

where TP, TN, FP and, FN are true positive, true negative, false positive and false negative values, respectively.

Table 2. Metrics for the correct classifications of the STN-DBS state of individual scans.

Analysis Repetition	Accuracy	Sensitivity	Specificity	Precision
1	0.8902	0.9024	0.8780	0.8810
2	0.8171	0.8049	0.8293	0.8250
3	0.8902	0.9512	0.8293	0.8479
4	0.8293	0.8780	0.7805	0.8000
5	0.9512	0.9268	0.9756	0.9744
6	0.8658	0.8293	0.9024	0.8947
7	0.8780	0.8780	0.8780	0.8780
8	0.8049	0.7805	0.8293	0.8205
9	0.9146	0.9024	0.9268	0.9250
10	0.8902	0.8293	0.9512	0.9444
Mean	**0.8732**	**0.8683**	**0.8780**	**0.8791**

Note: Accuracy, sensitivity, specificity and precision values of the method to correctly classify the STN-DBS state of individual scans. Each row contains the efficacy measure values for each of the 10 "experiments." The last row shows the mean values of efficacy measures across "experiments."

In order to assess the functional significance of the PCA and PCA-FLDA results, representative measures were computed to characterize the first principal component (PC1) and the FLDA predictor scores. These two measures were used in correlational analyses with results of the previously published region-based analyses of global blood flow and with several clinical measures. The results of the PCA analysis were represented by the magnitude of a feature vector in the direction of first principal component (PC1). For the prediction of DBS-*on* and *off* state using PCA-FLDA, we utilized the prediction value calculated by equation (10).

Results

The combination of PCA and FLDA classified STN-DBS *on* and *off* cerebral blood flow images with a high degree of accuracy and specificity. To establish the reliability of this method, the analysis was repeated 10 times by randomly choosing training and testing sets of images. For each repetition, all the efficacy measures were calculated. The results of these iterations and mean efficacy values are presented in Table 2. On average, the PCA-FLDA method achieved an accuracy value of 0.87 with minimum value of 0.80 and a maximum accuracy value of 0.95. Representative composite images are presented in Figure 1, where the colors represent the direction of the discriminator (i.e. light blue to dark blue = increasingly negative, red to yellow = increasingly positive). It should be noted that positive discrimination indicating increased CBF values are widely distributed across the cerebellum, but at lower intensity values than are observed in supratentorial brain regions.

To place the present results in context of the previous report of global CBF increases,[1] relationships between several measures derived from the present analyses, the global changes reported previously, and demographic characteristics were evaluated. STN-DBS *on* – *off* difference scores for global blood flow were computed from the previously published results, and these difference scores were compared across scans with the first principal component score (PC1) as well as with several derived discriminator scores from the PCA-FLDA analysis using bivariate correlations. The PC1 scores for the STN-DBS *off* scans were negatively correlated with the whole brain change scores [$r = -0.264$; $p = 0.029$], indicating that in the *off* condition, the *on-off* global blood flow scores decreased as the PC1 *off* scores increased. The PC1 scores for the STN-DBS *on* scans were positively correlated with the global change scores [$r = 0.512$; $p < 0.001$], indicating that in the *on* condition, the *on-off* global blood flow scores increased as the PC1 *on* scores increased. This is depicted in Figure 2. Independent of whole brain change scores, PC1 appears to be a marker of blood flow, especially in in the DBS *on* condition. The PC1 on scores were highly correlated with the region-based whole brain values in the *on* condition ($r = 0.967$; $p < 0.001$), and the PC1 *off* scores demonstrated a smaller, significant correlation with the region-based whole brain values in the *off* condition ($r = 0.426$; $p < 0.001$). Using the PCA-FLDA discriminators, the global difference scores were negatively correlated with the discriminator scores only in the *off* condition [$r = -0.25$; $p = 0.038$].

With respect to subjects' behavior during scanning, in the STN-DBS *on* condition, the PC1 scores were correlated with pause duration during the speech tasks [$r = 0.436$; $p = 0.002$], similar to the previously reported relationship with global blood flow changes[1] and consistent with the effects of STN-DBS *on* pausing during spontaneous speech.[23] In this relationship, global CBF was interpreted as a surrogate marker for PD severity rather than playing a direct role in motor speech control.

For clinical variables, the total amplitude of STN-DBS electrical stimulation was positively correlated with PC1 values [$r = 0.25$; $p = 0.025$] and the PCA-FLDA discriminator scores [$r = 0.278$; $p = 0.012$] in the *off* condition. As there was no stimulation in the *off* condition, it appears that total amplitude was serving as a surrogate measure of PD severity. The total amplitude was also positively correlated with PC1 values in the *on* condition [$r = 0.348$; $p = 0.001$]. For several other clinical characteristics, significant

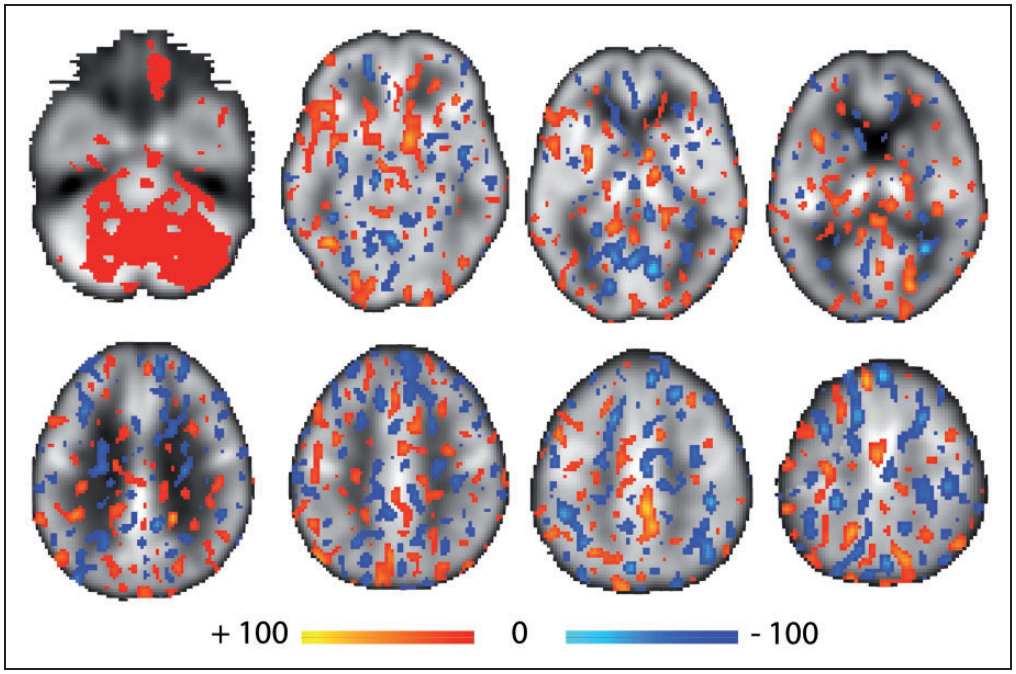

Figure 1. Representative brain slices color-coded to represent the results of the PCA-FLDA analysis. The discriminant scores are superimposed over the average of all 164 PET images. Discrimination pattern coefficients greater than 30% of the maximum absolute value (approximately two standard deviations from the mean) are shown. Red and blue colors indicate the positive (red to yellow = increasingly positive) and negative (light blue to dark blue = increasingly negative) coefficient values, respectively. One notable feature is the widespread distribution of positive discrimination values across the cerebellum, but at lower intensity values than in supratentorial brain regions.

correlations with PC1 and PCA-FLDA scores only occurred in the STN-DBS *off* condition. The duration of STN-DBS therapy was correlated with the PC1 values [$r = 0.335$; $p = 0.002$] and with the PCA-FLDA discriminator scores [$r = 0.289$; $p = 0.008$] in the *off* condition. The UPDRS motor scores were also correlated with the PC1 values [$r = 0.35$; $p = 0.001$] and PCA-FLDA discriminator scores [$r = 0.233$; $p = 0.035$] in the *off* condition. None of these clinical measures were correlated with the PC1 or PCA-FLDA discriminators scores in the *on* condition.

Discussion

The results of our voxel-based PCA-FLDA analysis revealed widespread changes in CBF as a function of STN-DBS status in individuals with PD. This procedure classified CBF PET images with respect to STN-DBS status during scanning with nearly 90% accuracy and specificity. An important point is that this level of discrimination was confirmed without having to estimate a normalization factor for intersubject global blood flow for these semi-quantitative CBF measures. The question of global blood flow normalization has caused some confusion in the literature on PD imaging, but it has been shown that network changes in the Parkinson's disease related profile (PDRP) are not an artifact of global changes.[24]

A comparison between the present and previous results provides some insights into STN-DBS effects. The whole-brain CBF *on* – *off* difference scores previously calculated using regions-of-interest[1] were positively correlated with the first principal component values for the STN-DBS *on* condition and negatively correlated with the first principal component values for the STN-DBS *off* condition. This relationship confirms the previously reported increase in global CBF during the STN-DBS *on* condition. However, the region-based global difference scores were only correlated with the PCA-FLDA discriminator values calculated for the STN-DBS *off* condition. The discrepancy between the PCA and PCA-FLDA relationships with whole-brain CBF suggests that while a global increase in CBF is a significant component of the STN-DBS effect, the accuracy and sensitivity of the PCA-FLDA are the result of more than just global changes. This discrepancy, together with the results of the clinical correlations with the PCA and PCA-FLDA results, suggests that CBF in the STN-DBS *on* and *off* conditions reflect different processes to some extent.

While the present study did not examine metabolism, an ^{18}F-fluorodeoxyglucose (FDG) PET study by

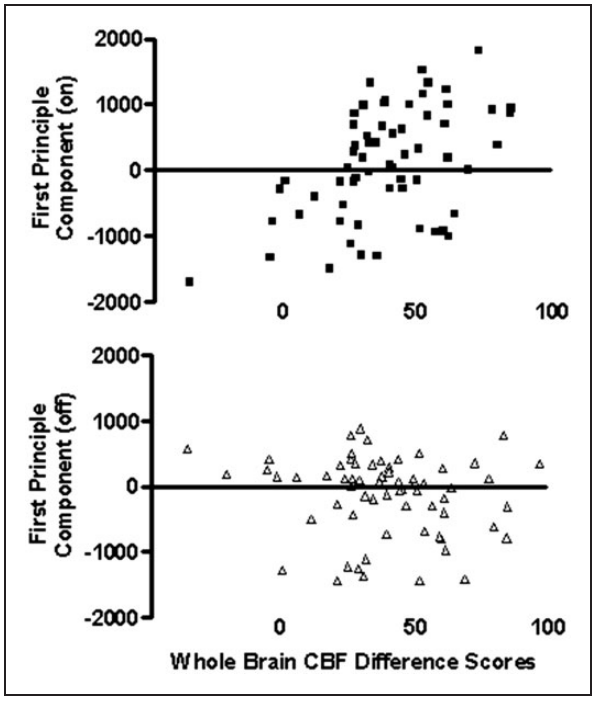

Figure 2. Scatter plots depicting the relationships between the STN-DBS *on* – *off* global CBF values (Sidtis et al.[1]) and the first principal component (PC1) values (present study) for the STN-DBS *on* and *off* conditions. The PC1 scores for the STN-DBS *on* scans were positively correlated with the global CBF change scores [$r = 0.512$; $p < 0.001$], indicating that PC1 scores increased as global CBF blood increased in the *on* condition. The opposite relationship between PC1 and global CBF difference scores [$r = -0.264$; $p = 0.029$] was observed in the STN-DBS *off* condition.

Garraux et al.[10] may be relevant to the present findings. Eight PD subjects were studied off medication in both STN-DBS *on* and *off* conditions during a resting state. Absolute quantitative data were not obtained, but images were normalized using brain areas that did not change as a function of STN-DBS status. Whole-brain values were obtained using large regions of interest. Their analysis indicated that whole-brain FDG uptake increased by approximately 11% when STN-DBS *on* was compared to *off*. Normalizing for these whole brain differences, multiple cortical and subcortical areas also increased with STN-DBS *on*, but no areas were found to decrease. With respect to regional changes associated with STN-DBS, Garraux et al. pointed out that the published results are inconsistent, with one likely cause being differences in the ways in which regional data were normalized for global effects. The range of sometimes conflicting regional changes associated with STN-DBS is reviewed by Garraux et al. so they will not be revisited in this paper.

The relationships between cerebral glucose metabolism and CBF following levodopa administration or STN-DBS treatment were examined by Hirano et al.[25] A voxel-based pattern analysis revealed increased CBF but decreased glucose metabolism with the administration of levodopa in a previously established PD related network (PDRP). Similar local dissociations were noted in multiple brain areas using a regional approach. The dissociation between CBF and glucose metabolism with the administration of levodopa was not observed during STN-DBS.

Although not explicitly addressing the question of whole-brain CBF changes with STN-DBS, two single photon emission-computed tomography (SPECT) studies revealed bilateral, large, multi-region CBF increases. Sestini et al.[26] studied 10 PD subjects, off medication, at rest. They did not evaluate possible whole-brain CBF changes, instead scaling all of the scans across conditions to a common global value (50 mL/100 mL per minute). Nevertheless, they found widespread bilateral increases in CBF when STN-DBS *on* values were compared to pre-operative and STN-DBS *off* conditions. Nagai et al.[27] studied a large group of STN-DBS subjects ($N = 92$) with SPECT. The subjects were divided into groups based on their UPDRS part III scores off medication. Whole-brain changes were not explicitly considered in their analysis either, but as in the Sestini et al.[26] study, widespread bilateral CBF increases were reported after STN-DBS, with the largest increases found in the subgroup with the best clinical outcome. In both SPECT studies, the DBS effects on CBF were anatomically extensive.

While the studies that address whole-brain changes with STN-DBS are limited, the available evidence suggests that such changes are neurophysiologically meaningful. Just as the therapeutic mechanisms of STN-DBS remains unclear, so are the mechanisms of STN-DBS global CBF changes. Leenders et al.[28] examined the question of whether the increased CBF following administration of levodopa was related to increased oxygen metabolism. Using ^{15}O PET, they measured CBF and oxygen metabolism in PD and normal subjects. Glucose metabolism was not measured. Both participant groups demonstrated increased CBF but no increase in oxygen metabolism, suggesting that the levodopa-induced CBF increases were not driven by changes in oxidative metabolism. In the PD group, CBF increased by 13% in the cortex and 20% in the basal ganglia, with smaller increases in the non-PD control group. Leenders et al. argued that these results were consistent with the available human and animal evidence indicating that stimulation of the dopaminergic system with dopaminergic agonists or levodopa increased CBF. As levodopa is a vasoactive substance that is associated with both vasoconstriction and vasodilation,[29–32] it appears that the dopaminergic system

could be a candidate for a role in whole-brain CBF changes during STN-DBS.

Stimulation of astrocytes during STN-DBS is another possible mechanism for global CBF changes.[7–9] Astrocytes play a significant role in the regulation of CBF, especially at the microvascular level, and may regulate CBF independent of metabolic demand.[33–35] The involvement of astrocytes in the effect of STN-DBS on CBF provides a mechanism for widespread brain changes and expands the palate of potential vasoactive substances beyond levodopa.

The present study suggests that STN-DBS produces a global increase in CBF, as reflected in the PC1 measure, as well as local or regional changes and network alterations, as inferred but not identified by the PCA-FLDA measures and the existing literature. Network changes do occur in these data, however, as we have identified functionally significant speech-specific cortical-subcortical changes independent of the global CBF effect.[36] The results of this study, together with the existing literature, raise several important questions. Does STN-DBS alter functional hyperemia and cerebral autoregulation? In this study, the discriminators derived from the PCA and the PCA-FLDA analyses were correlated to clinical measures in the STN-DBS *off* condition, but not the *on* condition. This dissociation may reflect the observation by Leenders et al.[28] that CBF increases following levodopa administration were not associated with corresponding changes in oxidative metabolism. The relationships between CBF and glucose metabolism appear to be different.[25]

Conclusions

STN-DBS is a clinically effective tool in the treatment of PD, but the therapeutic mechanisms remain unknown. We have previously reported significant increases in global CBF with STN-DBS in the *on* state, and the present PCA results support that observation. However, the high accuracy and specificity of the PCA-FLDA method in discriminating *on* and *off* conditions, while not completely capturing the whole-brain CBF increases, indicate that STN-DBS effects are more than global. Further, the observations that the CBF measures derived from the PCA-FLDA analysis were correlated with clinical measures in the STN-DBS *off* condition but not the *on* condition suggests some degree of dissociation between STN-DBS CBF increases and normal cerebrovascular principals like functional hyperemia and cerebral autoregulation. The identification of both global and local CBF changes associated with STN-DBS suggests a broader, albeit more complicated, approach to understanding its therapeutic mechanisms. The effects of STN-DBS will likely require characterizations in regional, network, and global domains.

Funding

This work was supported by NIH R01 DC 007658.

Acknowledgements

A preliminary version of this analytic approach was developed and presented by the late Ali Tabesh at the IXth International Conference on Quantification of Brain Function with PET.[37] The comments of Diana Sidtis on this manuscript are greatly appreciated as was the assistance of the members of the Brain and Behavior Laboratory and David Bjelke and Yilong Ma at the Feinstein Institute.

Declaration of conflicting interests

The author(s) declared no potential conflicts of interest with respect to the research, authorship, and/or publication of this article.

Authors' contributions

JJS and VD were directly involved in acquiring PET images. AMM and BA carried out the image processing and data analysis in consultation with JJS. MT and RA provided neurological and neurosurgical information on the subjects. DE provided oversight of image acquisition and initial image processing as well as contributing to the intellectual content of the manuscript.

References

1. Sidtis JJ, Tagliati M, Alterman R, et al. Therapeutic high-frequency stimulation of the subthalamic nucleus in Parkinson's disease produces global increases in cerebral blood flow. *J Cereb Blood Flow Metab* 2012; 32: 41–49.
2. Vitek JL. Deep brain stimulation: how does it work? *Cleve Clin J Med* 2008; 75(Suppl 2): S59–65.
3. Benabid AL, Chabardes S, Mitrofanis J, et al. Deep brain stimulation of the subthalamic nucleus for the treatment of Parkinson's disease. *Lancet Neurol* 1999; 8: 67–81.
4. McIntyre CC and Hahn PJ. Network perspectives on the mechanisms of deep brain stimulation. *Neurobio Dis* 2010; 38: 329–337.
5. Perlmutter JS and Mink JW. Deep brain stimulation. *Annu Rev Neurosci* 2006; 29: 229–257.
6. Montgomery EB and Gale JT. Mechanisms of action of deep brain stimulation (DBS). *Neurosci Biobehav Rev* 2008; 32: 388–407.
7. Tawfik VL, Chang S-Y, Hitti FL, et al. Deep brain stimulation results in local glutamate and adenosine release: investigation into the role of astrocytes. *Neurosurgery* 2010; 67: 367–375.
8. Vedam-Mai V, van Battum EY, Kamphuis W, et al. Unravelling the actions of deep brain stimulation: potential role for astrocytes. *Mol Psychiatry* 2012; 17: 124–131.
9. Fenoy AJ, Goetz L, Charbardes S, et al. Deep brain stimulation: are astrocytes a key driver behind the scene? *CNS Neurosci Ther* 2014; 20: 191–201.

10. Garraux G, Bahri MA, Lemaire C, et al. Brain energization in response to deep brain stimulation of subthalamic nuclei in Parkinson's disease. *J Cereb Blood Flow Metab* 2011; 31: 1612–1622.
11. Manrique M, Alborch E and Delgado JMR. Cerebral blood flow and behavior during brain stimulation in the goat. *Am J Physiol* 1977; 232: H495–H499.
12. Sun M-K and Reis DJ. Hypoxic excitation of medullary vasomotor neurons in rats are not mediated by glutamate or nitric oxide. *Neurosci Lett* 1993; 157: 219–222.
13. Ángyán L and Ángyán Z. Subthalamic influences on the cardiorespiratory functions in the cat. *Brain Res* 1999; 847: 130–133.
14. Golanov EV, Ruggiero DA and Reis DJA. Brainstem area mediating cerebrovascular and EEG responses to hypoxic excitation of rostral ventrolateral medulla in rat. *J Physiol* 2000; 529: 413–429.
15. Golanov EV, Christensen JRC and Reis DJ. Neurons of a limited subthalamic area mediate elevations in cortical cerebral blood flow evoked by hypoxia and excitation of neurons of the rostral ventrolateral medulla. *J Neurosci* 2001; 21: 4032–4041.
16. Ardekani BA, Strother SC, Anderson JR, et al. On detection of activation patterns using principal component analysis. In: Carson RE, Herscovitch P and Daube-Witherspoon ME (eds) *Quantitative functional brain imaging with positron emission tomography*. San Diego: Academic Press, 1998, pp.253–260.
17. Ceballos-Baumann AO, Boecker H, Bartenstein P, et al. A positron emission tomographic study of subthalamic nucleus stimulation in Parkinson disease. *Arch Neurol* 1999; 56: 997–1003.
18. Payoux P, Remy P, Damier P, et al. Subthalamic nucleus stimulation reduces abnormal motor cortical overactivity in Parkinson disease. *Arch Neurol* 2004; 61: 1307–1313.
19. Karimi M, Golchin N, Tabbal D, et al. Subthalamic nucleus stimulation-induced regional blood flow responses correlate with improvement of motor signs in Parkinson's disease. *Brain* 2008; 131: 2710–2719.
20. Sidtis JJ, Gomez C, Groshong A, et al. Mapping cerebral blood flow during speech production in hereditary ataxia. *Neuroimage* 2006; 31: 46–254.
21. Jackson JE. *A user's guide to principal components*. New York: John Wiley & Sons, Inc., 1991.
22. Strother SC, Anderson JR, Schaper KA, et al. Linear models of orthogonal subspaces and activated networks from functional activation PET studies of the human brain. In: Bizais Y, Barillot C and Di Paola R (eds) *Computational imaging and vision*. Dordrecht, Netherlands: Kluwer Academic Publishers, 1995, pp.299–310.
23. Ahn JS, Van Lancker Sidtis D and Sidtis JJ. Effects of deep brain stimulation on pausing during spontaneous speech in Parkinson's disease. *J Med Speech Lang Pathol* 2014; 21: 179–186.
24. Dhawan V, Tang CC, Ma Y, et al. Abnormal network topographies and changes in global activity: absence of a causal relationship. *Neuroimage* 2012; 63: 1827–1832.
25. Hirano S, Asanuma K, Ma Y, et al. Dissociation of metabolic and neurovascular responses to levodopa in the treatment of Parkinson's disease. *J Neurosci* 2008; 28: 4201–4209.
26. Sestini S, di Luzio AS, Ammannati F, et al. Changes in regional cerebral blood flow caused by deep-brain stimulation of the subthalamic nucleus in Parkinson's disease. *J Nucl Med* 2002; 43: 725–732.
27. Nagai T, Kajita Y, Maesawa S, et al. *Neurol Med Chir* 2012; 52: 865–872.
28. Leenders KL, Wolfson L, Gibbs JM, et al. The effects of L-dopa on regional cerebral blood flow and oxygen metabolism in patients with Parkinson's disease. *Brain* 1985; 108: 171–191.
29. Iadecola C. Neurogenic control of the cerebral microcirculation: is dopamine minding the store? *Nat Neurosci* 1998; 1: 263–265.
30. Iadecola C. Neurovascular regulation in the normal brain and in Alzheimer's disease. *Nat Rev Neurosci* 2004; 5: 347–360.
31. Drake CT and Iadecola C. The role of neuronal signaling in controlling cerebral blood flow. *Brain Lang* 2007; 102: 141–152.
32. Murphy MB. Dopamine: a role in the pathogenesis and treatment of hypertension. *J Hum Hypertens* 2000; 14(Suppl 1): S47–S50.
33. Takano T, Tian G-F, Peng W, et al. Astrocyte-mediated control of cerebral blood flow. *Nat Neurosci* 2006; 9: 260–265.
34. Iadecola C and Nedergaard M. Glial regulation of the cerebral microvasculature. *Nat Neurosci* 2007; 10: 1369–1376.
35. Filosa JA and Iddings JA. Astrocyte regulation of cerebral vascular tone. *Am J Physiol Heart Circ Physiol* 2013; 305: H609–H619.
36. Sidtis JJ, Sidtis D, Tagliati M, et al. Stimulation of the subthalamic nucleus in Parkinson's disease changes the relationship between regional cerebral blood flow and speech rate. *Stem Spraak Taalpathol* 2011; 17: 102.
37. Tabesh A, Ardekani B, Tagliati M, et al. Whole-brain PET study of Parkinson's patients reveals a complex pattern of rCBF changes associated with deep brain stimulation. *J Cereb Blood Flow Metab* 2009; 29: S280–S281.
38. Hoehn MM and Yahr MD. Parkinsonism: onset, progression, and mortality. *Neurology* 1967; 17: 427–442.